

In-phase vortex flow and superradiance in a Josephson superlattice embedded in a waveguide

A. V. Chiginev* and V. V. Kurin

Institute for Physics of Microstructure of the Russian Academy of Science, GSP-105, 603950 Nizhny Novgorod, Russia

(Received 25 December 2003; revised manuscript received 9 April 2004; published 23 December 2004)

We study the dynamics of a Josephson vortex lattice in a stack of long Josephson junctions electromagnetically connected with a waveguide in the form of a stripline. The stability of the dense rectangular vortex lattice is investigated analytically. We show that this regime appears to be stable provided the characteristic velocity of the symmetric perturbation mode in the system is lowest compared with other modes. We find a range of velocities at which the rectangular Josephson vortex lattice is stable. We perform a numerical experiment which shows a spontaneous establishing of the rectangular Josephson vortex lattice as the system parameters are changed.

DOI: 10.1103/PhysRevB.70.214523

PACS number(s): 74.78.Fk, 74.50.+r

I. INTRODUCTION

The idea of using the Josephson effect for generation of high-frequency electromagnetic oscillations has attracted the attention of many researchers since its discovery in 1962. The main advantages of Josephson junctions (JJ's) as oscillators are their small dimensions, good tunability, and possibility of working with frequencies up to several hundred GHz.¹ However, the radiation power of a single JJ is very small and insufficient for most applications. Combining JJ's into arrays could significantly increase the radiation power and reduce the linewidth of such devices. Multilayer Josephson structures provide good example of JJ arrays. At present, the existing technology allows growing high-quality multilayers such as Nb/Al-AIO_x/Nb stacks.² The interest to multilayer structures has become even greater after the discovery of intrinsic Josephson effect in highly anisotropic high-temperature superconductors.³ This discovery showed that some high-temperature superconductors (HTSC's), for example, Bi₂Sr₂CaCu₂O_{8+x}, may be treated as JJ stacks formed on atomic scales. Recent experiments showed the possibility of using Bi₂Sr₂CaCu₂O_{8+x} crystals as bases for high-frequency electronic devices.⁴

Electromagnetic radiation in multilayer structures can be produced by moving Josephson vortex lattice (JVL). The radiation is generated when a vortex collides with the edge of the stack. This principle is similar to the one used in the Josephson flux-flow oscillator⁵ (FFO) and, in this sense, a multilayer structure is essentially an arrangement of several Josephson FFO's, joined together in a stack. The maximal radiation power from such a structure is achieved when the vortices form a rectangular JVL, which is also referred to as the in-phase regime of vortex flow. In this case, the radiation power at the main harmonic is proportional to N^2 , where N is the number of layers in the stack. There are many publications devoted to investigations of stability of regular Josephson vortex structures in layered systems. It was shown in some papers that either the in-phase regime⁶ or the regime close to the in phase⁷ is reachable in Josephson stacks. However, these regimes have not been observed in experiments. Apparently, the rectangular JVL is unstable due to mechanisms which have not been taken into account so far in these

models, and the existence of instabilities is the intrinsic property of isolated Josephson stacks. However, one may expect that by changing the parameters of an external electromagnetic environment, for example, a waveguide or a cavity, it is possible to control the stability properties of the in-phase regime and reach stability of the rectangular JVL. It is well known that the connection of an external passive load to a Josephson junction chain essentially influences the condition of synchronization between these junctions (see Ref. 8 and later works⁹).

In the present paper we investigate the dynamics of Josephson vortices in a stack of long JJ electromagnetically coupled with a stripline, which is one of the simplest examples of electromagnetic environment. Such a system has several attractive features. First, it can be easily fabricated and used in an experiment. Second, as we show below, this system can be described in the framework of a simple model—a set of equations of the sine-Gordon type supplemented with terms responsible for the additional “global” coupling via the stripline. We analyze the stability of a rectangular JVL by the method used in our previous article.¹⁰ Using this approach, we show that the important factor which affects the stability of a JVL is the relation between the characteristic velocities of perturbation modes in the system. In particular, to ensure stability of a rectangular JVL, the symmetric perturbation mode must be the slowest one in the system. We show that under this condition the in-phase regime is stable in a certain range of the external current and, moreover, the in-phase regime is established spontaneously at these currents.

The article is organized as follows. In Sec. II we derive a set of equations describing a JJ stack connected with a stripline. Section III is devoted to analytical investigation of stability of the in-phase regime of vortex motion in the system under consideration. The method and results of the numerical experiment are described in Sec. IV. Finally, the main results of the work are formulated in the summary.

II. BASIC EQUATIONS: INFLUENCE OF EXTERNAL WAVEGUIDE SYSTEM

Let us consider a stacked configuration of JJ's built in an external waveguide system. For simplicity, we choose a

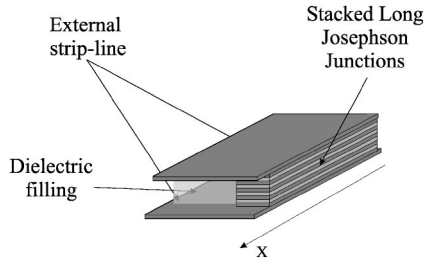


FIG. 1. View of a Josephson superlattice globally coupled via external stripline.

simple stripline as the waveguide. The configuration of junctions and external stripline is shown in Fig. 1.

The multilayer Josephson structure is usually described by a set of sine-Gordon-type equations supplemented with terms responsible for the interlayer coupling. This coupling is provided by various mechanisms such as magnetic coupling,^{11,12} charge coupling,¹³ quasiparticle imbalance,¹⁴ etc. To demonstrate our approach, we consider a simple model with magnetic coupling. For the sake of simplicity we neglect the in-plane dissipation.⁷

Assuming that superconductor superlattice is homogeneous and, hence, its parameters do not depend on the layer index, we write down a set of equations describing a JJ stack as

$$\sum_{m=1}^N K_{mn} \{ \partial_t^2 \varphi_m + \gamma \partial_t \varphi_m + \sin \varphi_m - j \} = \partial_x^2 \varphi_n, \quad n = 1, \dots, N, \quad (1)$$

where φ_n is the Josephson phase difference in the n th JJ, $\partial_{t,x}$ are the differentiating operators with respect to time and coordinate, respectively, γ is the damping coefficient, j is the density of a current flowing from the external waveguide, the dimensionless time t and coordinate x are normalized to the Josephson plasma frequency ω_J , and the Josephson characteristic length λ_J is defined as

$$\omega_J^2 = \frac{8\pi e d' j_c}{\hbar \epsilon} \quad \text{and} \quad \lambda_J = V_s / \omega_J,$$

where

$$V_s = \frac{c}{\sqrt{\epsilon}} \left[\frac{d' \sinh(t/\lambda)}{d' \sinh(t/\lambda) + 2\lambda (\cosh(t/\lambda) - 1)} \right]^{1/2}$$

is the Swihart velocity, c is the light speed, d' and t are thicknesses of the insulator and inner superconductor layers, respectively, λ is the London penetration depth, and ϵ is the dielectric constant.

The matrix K_{mn} with dimensions $N \times N$ describes coupling between the neighboring junctions via magnetic field penetration through the superconducting layer. The matrix elements K_{mn} are determined by layers thicknesses and magnetic field penetration depth¹¹

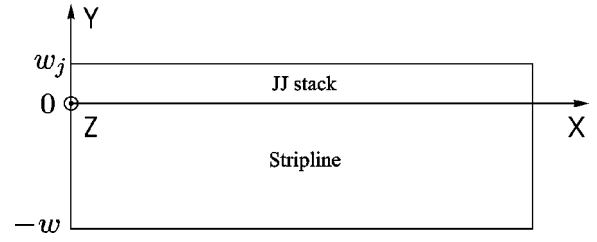


FIG. 2. To the derivation of the set of Eqs. (16). Top view of the multilayer structure connected with a stripline. The coordinate system is shown.

$$K_{ii} = 1 - 2s, \quad i = 2, \dots, N-1,$$

$$K_{11} = K_{NN} = \frac{d' + \lambda \coth(t/\lambda) + \lambda \coth(t_{ext}/\lambda)}{d' \sinh(t/\lambda) + 2\lambda [\cosh(t/\lambda) - 1]},$$

$$K_{i,i\pm 1} = s, \quad (2)$$

where

$$s = - \frac{\lambda}{d' \sinh(t/\lambda) + 2\lambda [\cosh(t/\lambda) - 1]} \quad (3)$$

characterizes inductive coupling between the layers in the superlattice, and t_{ext} is the thickness of the outer superconducting layer. In the present paper we assume the parameters of the inner layers to be the same, and the thicknesses of the outer layers t_{ext} to be chosen so that the elements K_{11} , K_{NN} are equal to

$$K_{11} = K_{NN} = 1 - s. \quad (4)$$

There are two reasons for the choice of matrix K_{mn} in the form (4). First, the solution which describes the in-phase regime and has the same form in all junctions [see Eq. (17) later] exists only provided the condition (4) is fulfilled. Second, as shown below, it allows one to easily find the eigenvalues and eigenvectors of matrix (4) and, consequently, diagonalize it.

Current j from the stripline is defined by a total voltage on the Josephson stack $U = \partial_t \sum_n \varphi_n$ by the relation $j = \hat{Y}U$, where \hat{Y} is admittance of the external electro-dynamical system, and by external biasing current j_{ext} , which we assume to be injected into the edge of the stripline. It is convenient to write both contributions as

$$j = \hat{H}j_{ext} - \hat{G} \sum_{n=1}^N \varphi_n, \quad (5)$$

where \hat{G} is the operator expressing current via total phase difference, which is proportional to the admittance $\hat{Y} = \partial_t \hat{G}$, operator \hat{H} stands for diffuency of injected current within the stripline.

Now we briefly describe the derivation of the expression for the operators \hat{G} and \hat{H} for a simple stripline, following the procedure described in Ref. 15. We introduce the Cartesian coordinates as shown in Fig. 2. The distribution of current $\vec{I}(x, y, t)$ and voltage $U(x, y, t)$ within a passive stripline is described by ordinary telegraph equations:

$$L \partial_t \vec{I} + \vec{\nabla} U = \vec{0}, \quad (6)$$

$$C \partial_t U + \text{div } \vec{I} = 0; \quad (7)$$

here L, C are dimensionless inductance and capacity of the stripline, related to unit square and normalized to the respective values of Josephson junctions. Introducing a new scalar variable ψ by relation $U = \partial_t \psi$, we come to relation $\vec{I} = L^{-1} \vec{\nabla} \psi$ and a two-dimensional wave equation for ψ :

$$c_e^{-2} (\partial_t^2 + \Gamma \partial_t) \psi - \partial_x^2 \psi - \partial_y^2 \psi = 0, \quad (8)$$

where c_e and Γ are, respectively, the dimensionless velocity and the damping rate of electromagnetic waves in the stripline. On the boundaries with free space $y = -w$ and with a stack of JJ's $y = 0$ the conditions of current and voltage continuity

$$\begin{aligned} L^{-1} \partial_y \psi|_{y=-w} &= j_e w_j, & L^{-1} \partial_y \psi|_{y=0} &= j w_j, \\ \psi|_{y=0} &= \sum_{n=1}^N \varphi_n \end{aligned} \quad (9)$$

should be satisfied. Here we assume that bias current is injected in the edge $y = -w$ of a stripline. By solving the linear equation (8) with boundary conditions (9) we will find a formula expressing dependency of current j flowing into the Josephson stack, on Josephson phases φ_n . To this effect, we represent functions ψ, φ_n, j, j_e as Fourier integrals

$$\psi(x, y, t) = \int e^{-i\omega t + ikx} \psi_{\omega, k}(y) \frac{d\omega}{2\pi} \frac{dk}{2\pi}, \quad (10)$$

which lead us to one-dimensional differential equation for $\psi_{\omega, k}(y)$

$$\partial_y^2 \psi - \kappa^2 \psi = 0, \quad (11)$$

where we introduce $\kappa(\omega, k) = \sqrt{k^2 - \omega(\omega + i\Gamma)/c_e^2}$ and omit, for brevity, the subscribe ω, k . A general solution of Eq. (11) is

$$\psi = A \cosh \kappa(y + w) + B \sinh \kappa(y + w), \quad (12)$$

whence, satisfying the boundary conditions ((9)) and finding A, B we come to the relations

$$j(\omega, k) = H(\omega, k) j_e(\omega, k) - G(\omega, k) \sum_{n=1}^N \varphi_n(\omega, k), \quad (13)$$

expressing dependency of current j flowing into the Josephson superlattice, on phase distribution $\sum_n \varphi_n$ and injected current j_e in the Fourier representation. Functions $G(\omega, k), H(\omega, k)$ are defined as

$$H(\omega, k) = \frac{1}{\cosh \kappa w}, \quad G(\omega, k) = \frac{w}{w_j L} \frac{\kappa}{\tanh \kappa w}. \quad (14)$$

Returning in Eq. (14) to the (x, t) representation, we find relations expressing $j(x, t)$ via $j_e(x, t)$ and $\sum_n \varphi_n(x, t)$. Note that for a narrow stripline, when the condition $\kappa w \ll 1$ is fulfilled, operator \hat{H} turns to 1 and \hat{G} turns to the wave operator

$$\hat{G} = \alpha (c_e^{-2} \partial_t^2 + c_e^{-2} \Gamma \partial_t - \partial_x^2), \quad (15)$$

where we introduce the value

$$\alpha = \frac{w}{w_j L}$$

defining the strength of coupling between the Josephson superlattice and the external stripline. Further we use expression (15) for operator \hat{G} .

Thus, finally, we may conclude that the Josephson superlattice with intrinsic coupling globally coupled via a narrow external strip line is described by the following set of equations:

$$\begin{aligned} \sum_{m=1}^N K_{mn} \left\{ \partial_t^2 \varphi_m + \gamma \partial_t \varphi_m + \sin \varphi_m - j_e + \hat{G} \sum_l \varphi_l \right\} &= \partial_x^2 \varphi_n, \\ n &= 1, \dots, N, \end{aligned} \quad (16)$$

where operator \hat{G} is defined by relation (15). Equations describing intrinsic coupling of different nature, say, charge and quasiparticle coupling, and taking into account the in-plane dissipation, may be derived in a similar way.

III. ANALYSIS OF THE RECTANGULAR JVL STABILITY

In this section we perform an analytical investigation of stability of the solution to set (16) which describes the in-phase regime of vortex flow in the system. The set of equations (16) has a solution describing the rectangular JVL. In the limit of a high external magnetic field it can be written as

$$\varphi_n^0 \equiv \varphi^0 = h(x - ut) + \text{Im} \frac{e^{ih(x-ut)}}{\mathcal{L}}, \quad (17)$$

where h is the dimensionless external magnetic field and

$$\mathcal{L} = -h^2 [(1 - u^2) + \alpha N (1 - u^2/c_e^2)] + ihu \gamma_e. \quad (18)$$

The JVL velocity u depends on the external current via the energy balance condition¹⁶

$$j_e + hu \gamma_e = \frac{1}{2} \text{Im} \frac{1}{\mathcal{L}}. \quad (19)$$

Note again that the solution in the form (17) exists only provided the matrix \hat{K} satisfies the condition (4).

In order to investigate the stability of the JVL φ^0 , we search the solution of Eq. (16) in the form

$$\varphi_n(x, t) = \varphi^0 + \psi_n(x, t), \quad (20)$$

where $|\psi_n| \ll 1$. The set of equations for perturbations ψ_n is written as follows:

$$\partial_x^2 \psi_n = \sum_{m=1}^N K_{mn} \left(\partial_t^2 \psi_n + \gamma \partial_t \psi_n + \cos \varphi^0 \psi_n + \hat{G} \sum_{l=1}^N \psi_l \right), \quad (21)$$

where $\cos \varphi^0 \approx \cos h(x - ut) - \text{Re} [1 - \exp 2ih(x - ut)]/2\mathcal{L}$.

The specific choice of matrix \hat{K} elements in the form (4) allows us to use a cosine Fourier transform to diagonalize the matrix. After applying the cos-transform

$$\psi_n = N^{-1} \left(\chi_1 + 2 \sum_{l=2}^N \chi_l \cos \left(n - \frac{1}{2} \right) (l-1) \frac{\pi}{N} \right), \quad (22a)$$

$$\chi_l = \sum_{n=1}^N \psi_n \cos \left(n - \frac{1}{2} \right) (l-1) \frac{\pi}{N} \quad (22b)$$

to the set of Eqs. (21) we obtain N -independent equations for χ_l :

$$(1 + \alpha N) \partial_x^2 \chi_1 = \left(1 + \frac{\alpha N}{c_e^2} \right) \partial_t^2 \chi_1 + \gamma_e \partial_t \chi_1 + \cos \varphi^0 \chi_1, \quad (23a)$$

$$v_l^2 \partial_x^2 \chi_l = \partial_t^2 \chi_l + \gamma \partial_t \chi_l + \cos \varphi^0 \chi_l, \quad l = 2, \dots, N. \quad (23b)$$

Equations (23a) and (23b) are of the hyperbolic type. Equation (23a) describes the evolution of perturbations which are same in all layers (symmetric perturbations). The characteristic velocity in Eq. (23a)

$$v_1^2 = \frac{1 + \alpha N}{1 + \alpha N / c_e^2} \quad (24)$$

depends on the external stripline parameters. For $N-1$ Eqs. (23b) describe the asymmetric perturbations. The characteristic velocities in Eqs. (23b) are

$$v_l^2 = \frac{1}{1 - 2s[1 - \cos(l-1)\pi/N]}, \quad l = 2, \dots, N. \quad (25)$$

By changing the external stripline parameters, we can control the value of the symmetric mode velocity v_1 , while the characteristic velocities of other modes remain unchanged. The spectrum of characteristic velocities of linear perturbation modes is shown in Fig. 3. Due to the fact that the set of equations for perturbations has been reduced to N separate equations we may investigate the stability of φ^0 with respect to each perturbation χ_l individually. For the stability analysis we use the method described in Ref. 10.

A. Symmetric perturbations

We start with the investigation of stability of the rectangular JVL with respect to symmetric perturbations χ_1 which are described by Eq. (23a). To solve Eq. (23a) we use the Lorentz transform with the velocity not exceeding v_1 since it does not change the wave operator $v_1^2 \partial_x^2 - \partial_t^2$. Depending upon the relation between v_1 and the solution velocity u we change to the reference frame where the parameter in Eq. (23a) depends either on the coordinate (at $u < v_1$) or on the time (at $u > v_1$).

1. "Subluminal" case

First, we consider the case $0 < u < v_1$. We perform Lorentz transformation in (23a) with simultaneous rescaling of the coordinate and time,

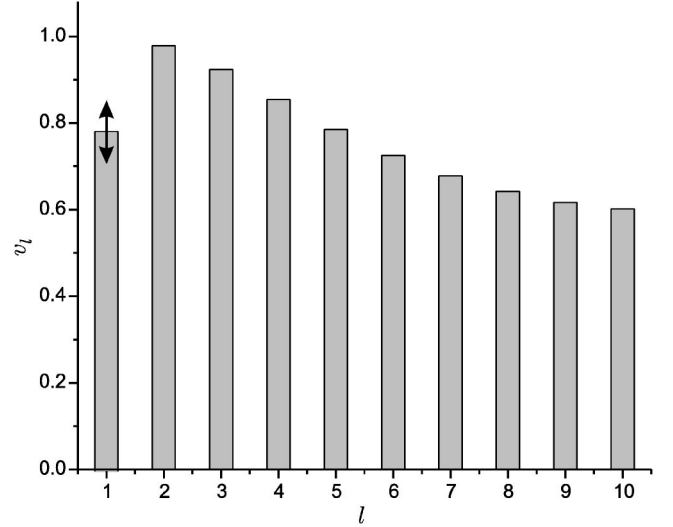


FIG. 3. The spectrum of characteristic velocities of linear perturbation modes vs mode number for the case $N=10$. By changing the parameters of the external stripline, one controls the velocity of symmetric perturbation v_1 not touching the velocities of other modes.

$$\xi = \frac{h}{2}(x - ut), \quad (26a)$$

$$\tau = \frac{h}{2} \left(t - \frac{u}{v_1^2} x \right). \quad (26b)$$

The equation takes the following form in new variables:

$$\begin{aligned} \chi_{1\xi\xi} - v_1^{-2} \chi_{1\tau\tau} &= \frac{2}{h} \frac{\gamma_e}{1 + \alpha N} \frac{1}{1 - u^2/v_1^2} (\chi_{1\tau} - u \chi_{1\xi}) \\ &+ \frac{4}{h^2} \frac{1}{1 - u^2/v_1^2} \frac{1}{1 + \alpha N} \left(\cos 2\xi - \frac{1}{2} \text{Re} \frac{1}{\mathcal{L}} \right) \chi_1. \end{aligned} \quad (27)$$

The coefficient at χ_1 in this equation depends only on the new coordinate ξ . As the coefficients in Eq. (27) are independent of τ , we may apply the Fourier transform to χ_1 which yields

$$\begin{aligned} \tilde{\chi}'' + \frac{\omega^2}{v_1^2} \tilde{\chi} &= \frac{2}{h} \frac{\gamma_e}{1 + \alpha N} \frac{1}{1 - u^2/v_1^2} (-i\omega \tilde{\chi} - u \tilde{\chi}') \\ &+ \frac{4}{h^2} \frac{1}{1 - u^2/v_1^2} \frac{1}{1 + \alpha N} \left[\cos 2\xi - \frac{1}{2} \text{Re} \frac{1}{\mathcal{L}} \right] \tilde{\chi}, \end{aligned} \quad (28)$$

where $\theta(\omega, \xi) = \int_{-\infty}^{\infty} \chi_1(\tau, \xi) \exp(i\omega\tau) d\tau$. Let us write down this equation in new variables:

$$\theta'' + 2\delta\theta' - \mu \cos(2\xi)\theta = \Omega^2\theta, \quad (29)$$

where $\mu = 4h^{-2}(1 - u^2/v_1^2)^{-1}(1 + \alpha N)^{-1}$, $\delta = h^{-1}\gamma_e(1 + \alpha N)^{-1}u(1 - u^2/v_1^2)^{-1}$, $\Omega^2 = \omega^2 v_1^{-2} + 2i\omega\delta u^{-1} + (\mu/2)\text{Re}\mathcal{L}^{-1}$. According to the Bloch theorem, the solution of this equation has the form $\theta(\xi) = U_q(\xi) \exp iq\xi$, where $U_q(\xi)$ is a function

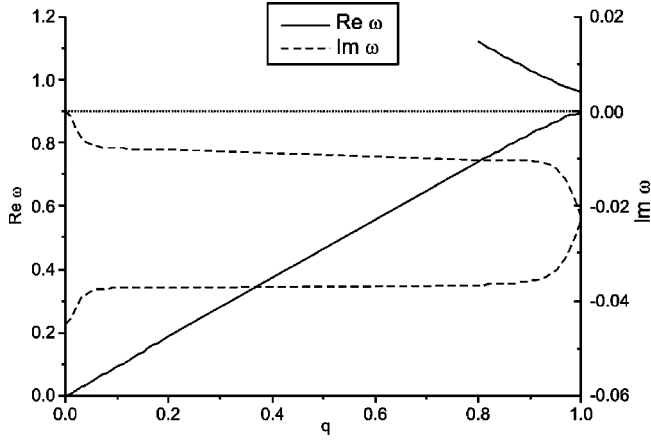


FIG. 4. The eigenfrequency spectrum $\omega(q)$ in the “subluminal” case.

with a period π and q is a quasimomentum. Assuming the parameter μ to be a small perturbation in this equation, we notice that the solution far from the Bragg resonances remains unperturbed and has the form of a harmonic function. Thus, the eigenfrequency spectrum is

$$\Omega^2(q) = q^2 - 2i\delta q. \quad (30)$$

In the vicinity of the middle part of the first Brillouin zone the solution has the form

$$\theta(\xi) = e^{iq\xi}(\theta_0 + \theta_2 e^{2i\xi} + \theta_{-2} e^{-2i\xi}), \quad (31)$$

where $\theta_{0,\pm 2}$ are constants. The eigenfrequency spectrum approximately equals

$$\Omega^2 = q^2 - 2i\delta q - \frac{\mu^2}{8} \frac{1}{1 - (q - i\delta)^2}. \quad (32)$$

In the vicinity of the first Brillouin zone edge we search for a solution in the form

$$\theta(\xi) = e^{iq\xi}(\theta_1 e^{i\xi} + \theta_{-1} e^{-i\xi}), \quad (33)$$

where $\theta_{\pm 1}$ are constants. The eigenfrequency spectrum is

$$\Omega_{1,2}^2 = 1 + q^2 - 2i\delta q \pm 2\sqrt{(q - i\delta)^2 + \frac{\mu^2}{16}}. \quad (34)$$

The dependence of eigenvalues ω on quasimomentum q is shown in Fig. 4. As seen in this figure, the imaginary part of ω does not take positive values at any q . Thus, there is no solution exponentially growing in time. Consequently, the rectangular JVL is stable with respect to symmetric perturbations in the “subluminal” case.

2. Superluminal case

Let us consider now the case $u > v_1$. As in the previous situation, we perform Lorentz transformation in Eq. (23a) but now with a velocity v_1^2/u (which is obviously less than v_1):

$$\xi = \frac{hu}{2} \left(x - \frac{v_1^2}{u} t \right), \quad (35a)$$

$$\tau = \frac{hu}{2} \left(t - \frac{x}{u} \right). \quad (35b)$$

The equation takes the following form in the new variables:

$$\begin{aligned} v_1^2 \chi_{1\xi\xi} - \chi_{1\tau\tau} = & \frac{2}{h} \frac{\gamma_e}{1 + \alpha N u^2/v_1^2 - 1} \frac{u}{u} \left(\chi_{1\tau} - \frac{v_1^2}{u} \chi_{1\xi} \right) \\ & + \frac{4}{h^2} \frac{1}{u^2/v_1^2 - 1} \frac{1}{1 + \alpha N} \left(\cos 2\tau - \frac{1}{2} \text{Re} \frac{1}{\mathcal{L}} \right) \chi_1. \end{aligned} \quad (36)$$

The coefficient in this equation depends only on the new time τ . We expand the perturbation χ_1 into a Fourier integral over ξ and obtain

$$\begin{aligned} -k^2 v_1^2 \tilde{\chi} - \tilde{\chi}'' = & \frac{2}{h} \frac{\gamma_e}{1 + \alpha N u^2/v_1^2 - 1} \frac{u}{u} \left(\tilde{\chi}' - \frac{v_1^2}{u} ik \tilde{\chi} \right) \\ & + \frac{4}{h^2} \frac{1}{u^2/v_1^2 - 1} \frac{1}{1 + \alpha N} \left(\cos 2\tau - \frac{1}{2} \text{Re} \frac{1}{\mathcal{L}} \right) \tilde{\chi}, \end{aligned} \quad (37)$$

where $\theta(k, \tau) = \int_{-\infty}^{\infty} \chi_1(\xi, \tau) \exp(-ik\xi) d\xi$. In new variables the equation is

$$\theta'' + 2\delta\theta' + \mu \cos(2\tau)\theta = -Q^2\theta, \quad (38)$$

where $\mu = 4h^{-2}(u^2/v_1^2 - 1)^{-1}(1 + \alpha N)^{-1}$, $\delta = h^{-1}\gamma_e(1 + \alpha N)^{-1}u(u^2/v_1^2 - 1)^{-1}$, $Q^2 = k^2 v_1^2 - 2ik\delta v_1^2 u^{-1} - (\mu/2)\text{Re} \mathcal{L}^{-1}$.

The solution of this equation has the form $\theta(\tau) = U_\varepsilon(\tau) \exp i\varepsilon\tau$, where $U_\varepsilon(\tau)$ is a function with a period π and ε is a quasienergy. Applying the same method as in the “subluminal” case, we obtain the eigenfrequency spectrum far from the Bragg resonances:

$$Q^2 = \varepsilon^2 + 2i\delta\varepsilon, \quad (39)$$

near the middle of the first Brillouin zone:

$$Q^2 = \varepsilon^2 + 2i\delta\varepsilon - \frac{\mu^2}{8} \frac{1}{1 - (\varepsilon + i\delta)^2}, \quad (40)$$

and near the edge of the first Brillouin zone:

$$\varepsilon_{1,2}^2 + 2i\delta\varepsilon = 1 + Q^2 \pm 2\sqrt{Q^2 + \frac{\mu^2}{16}}. \quad (41)$$

If the solution velocity u is slightly greater than v_1 , the quasienergy spectrum $\varepsilon(k)$ looks as in Fig. 5. It is seen that there is a region of k which corresponds to the positive imaginary part of the quasienergy. It means that there are perturbations exponentially growing in time, thus the in-phase regime is unstable at $u > v_1$. As the periodic coefficient in Eq. (37) depends only on time, this instability may be referred to as the parametric instability, by analogy with the phenomenon of parametric resonance.

As follows from formula (41), the spectrum $\varepsilon(k)$ changes qualitatively with an increase in the solution velocity u . The part of the spectrum corresponding to the vicinity of the first Brillouin zone edge is shown in Fig. 6. The region of k corresponding to $\text{Im} \varepsilon > 0$ disappears, which indicates suppres-

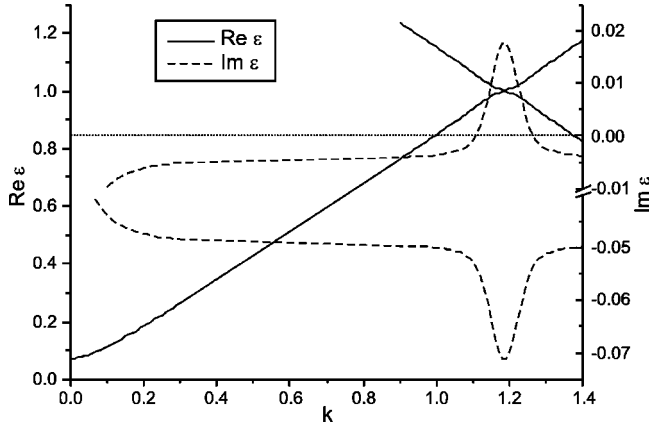


FIG. 5. The quasienergy spectrum $\varepsilon(k)$ in the “superluminal” case at $v_1 < u < v^*$.

sion of the parametric instability. It was shown in Ref. 10 that this suppression takes place provided $hu\gamma \geq 1$. This gives the estimate of the solution velocity above which the parametric instability is suppressed:

$$v^* \approx (h\gamma)^{-1}. \quad (42)$$

Hence, at $v_1 < u < v^*$ the solution describing the in-phase regime is parametrically unstable with respect to symmetric perturbations, while at $u > v^*$ the rectangular lattice becomes stable owing to the suppression of parametric instability.

B. Asymmetric perturbations

The remaining $N-1$ Eqs. (23b) for asymmetric perturbations $\chi_l, l=2, \dots, N$ have a structure similar to Eq. (23a), so, they can be analyzed in the same way as Eq. (23a) for symmetric perturbations. The characteristic velocities of Eqs. (23b) are $v_l, l=2, \dots, N$. In the subluminal case ($u < v_l$) Eq. (23b) is reduced to Eq. (29) with the parameters

$$\mu = 4h^{-2}(v_l^2 - u^2)^{-1}, \quad (43)$$

$$\Omega^2 = \frac{\omega^2}{v_l^2} + i\omega \frac{2\delta}{u} + \frac{\mu}{2} \text{Re} \frac{1}{\mathcal{L}}, \quad (44)$$

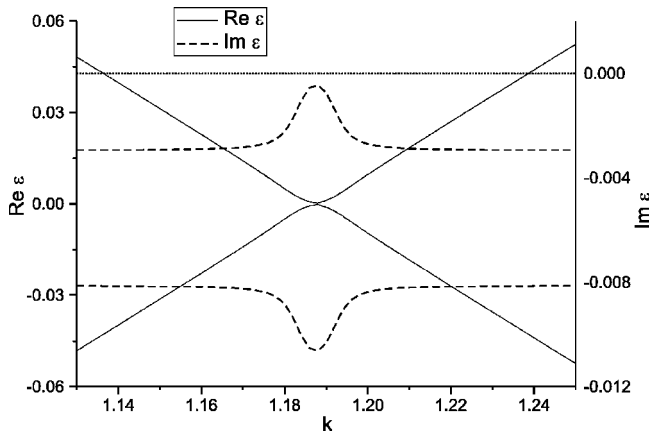


FIG. 6. A part of the quasienergy spectrum $\varepsilon(k)$ near the Brillouin zone edge in the “superluminal” case at $u > v^*$.

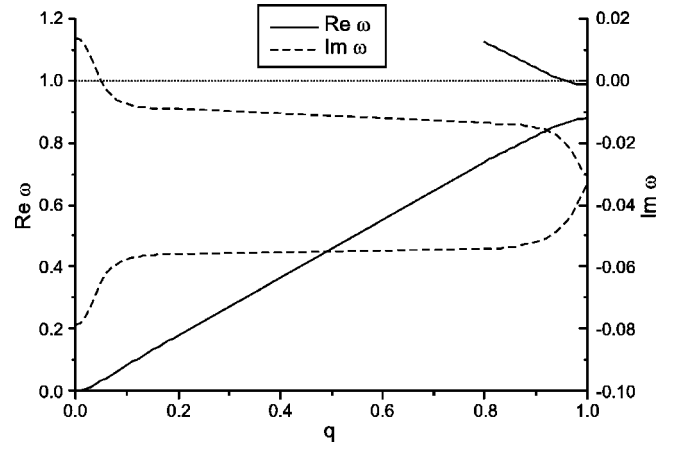


FIG. 7. The eigenfrequency spectrum $\omega(q)$ of asymmetric perturbations in the subluminal case at $u < v'$.

$$\delta = \frac{1}{h} \frac{\gamma u}{v_l^2 - u^2}. \quad (45)$$

In the superluminal case ($u > v_l$) it is reduced to Eq. (38) with the parameters

$$\mu = 4h^{-2}(u^2 - v_l^2)^{-1}, \quad (46)$$

$$Q^2 = k^2 v_l^2 + ik \frac{2\delta v_l^2}{u} + \frac{\mu}{2} \text{Re} \frac{1}{\mathcal{L}}, \quad (47)$$

$$\delta = \frac{1}{h} \frac{\gamma u}{u^2 - v_l^2}. \quad (48)$$

The solution of Eqs. (29) and (38) and perturbation spectra are described by formulas (30)–(34) and (39)–(41) (with the account of new expressions for the parameters).

Analyzing the eigenfrequency spectrum $\omega(q)$ in the subluminal case we arrive at the following conclusion. Provided the symmetric perturbations are slowest ($v_1 < v_l, l=2, \dots, N$), the spectrum $\omega(q)$ qualitatively depends on the relation between the JVL velocity u and a certain threshold value v' . If $u < v'$, the spectrum looks like in Fig. 7. There is a region of positive $\text{Im } \omega$ at small q , which is the evidence of long-wavelength instabilities in the system. Thus, the rectangular JVL is unstable at $u < v'$ —the vortex chains in the neighboring layers tend to shift forming a nonrectangular lattice. In the opposite case ($u > v'$) the spectrum $\omega(q)$ changes its form (Fig. 8). In this case, all asymmetric perturbations in the system are decaying, thus the rectangular JVL is stable with respect to asymmetric perturbations. The threshold value of JVL velocity v' at which the sign of $\text{Im } \omega$ changes can be found analytically in the limit of low dissipation

$$v'^2 = v_1^2 - \frac{(v_{\min}^2 - v_1^2)(v_1^2 - c_e^2)}{1 - v_1^2}, \quad (49)$$

where v_{\min} is the smallest characteristic velocity of asymmetric modes $v_l, l=2, \dots, N$. As seen from this formula, the value v' belongs to the region of the in-phase regime stabil-

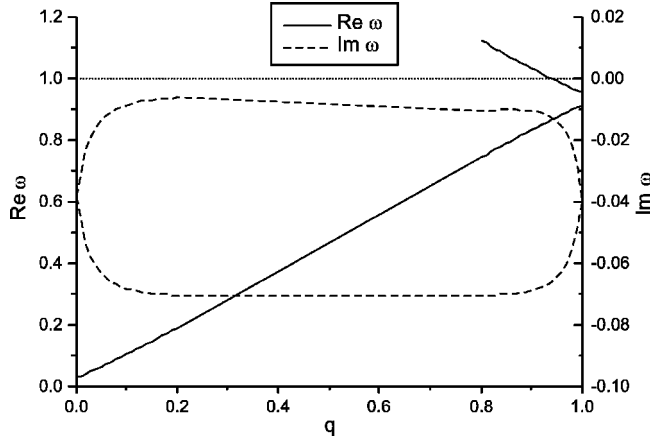


FIG. 8. The eigenfrequency spectrum $\omega(q)$ of asymmetric perturbations in the subluminal case at $u > v'$.

ity with respect to symmetric perturbations $0 < u < v_1$, provided $v_1 < v_l, l=2, \dots, N$. It means that only under this condition there is a region $v' < u < v_1$ where the rectangular JVL is stable with respect to all perturbations in the system.

In the superluminal case the quasienergy spectrum of asymmetric perturbations qualitatively depends on the solution velocity as in the case of symmetric perturbations. At $v_l < u < v^*, l=2, \dots, N$ the spectrum is similar to the one shown in Fig. 5, i.e., the parametric instability of the solution takes place. At $u > v^*$ the part of the spectrum near the first Brillouin zone edge looks like in Fig. 6, i.e., the parametric instability with respect to asymmetric perturbations appears to be suppressed.

C. Conclusion

Summing up the analytical results obtained above we come to the following conclusion. Provided the symmetric mode of perturbations is the slowest one in the system, the stability diagram looks like in Fig. 9. At JVL velocity $0 < u < v'$ the in-phase regime is unstable with respect to long-wave-length perturbations and this instability causes formation of a triangular lattice. At $v' < u < v_1$ the in-phase regime is stable. At $u > v_1$ the short-wave-length parametric instability is developed but further increase of the JVL velocity leads to suppression of this instability. If the symmetric mode is not the slowest one, then, as shown in Fig. 10, the region of the in-phase regime stability disappears and the regions of long-wave-length and short-wave-length instabilities overlap. Thus, the in-phase regime is unstable as long as the JVL velocity is high enough to suppress the parametric instability.

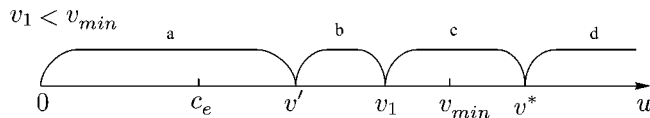


FIG. 9. The in-phase regime stability diagram at $v_1 < v_{min}$. Letters denote: a, region of long-wave-length instability; b, region of absolute stability; c, region of parametric instability; d, region with suppressed parametric instability.

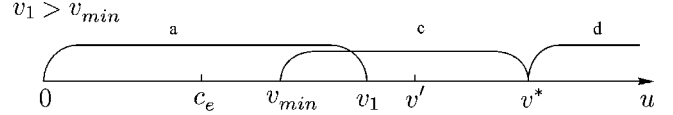


FIG. 10. The in-phase regime stability diagram at $v_1 > v_{min}$. The regions corresponding to different stability regimes are denoted as in Fig. 9.

IV. NUMERICAL EXPERIMENT

In the preceding section we have shown analytically that the rectangular JVL may be stable under certain conditions. In terms of applications it would be interesting to know whether this regime is established spontaneously when the system parameters are changed. The linear perturbation method is insufficient to check it, which calls for consideration of the nonlinear problem. To this end, we perform a numerical experiment which is described in the present section. Besides, the changes in the observed field distribution due to the instabilities in the system can be found by numerical simulation.

A. Method

Let us briefly describe the method of numerical experiment. For the sake of simplicity we assume the annular geometry of the system with a length L . It means that the phase in each layer of the stack satisfies the boundary condition

$$\varphi_n(L) = \varphi_n(0) + 2\pi R_n, \quad (50)$$

where R_n is the number of vortices trapped in the n th junction. Introducing new variables $\phi_n(x) = \varphi_n(x) - 2\pi R_n x/L$ satisfying the boundary conditions $\phi_n(L) = \phi_n(0)$, we come to a set of equations for ϕ_n

$$\sum_{m=1}^N K_{mn} \left\{ \partial_x^2 \phi_m + \gamma \partial_t \phi_m + \sin \left(\phi_m + \frac{2\pi R_m x}{L} \right) - j + \hat{G} \sum_{l=1}^N \phi_l \right\} = \partial_x^2 \phi_n, n = 1, \dots, N. \quad (51)$$

Applying the cos transform (22a) and (22b) to this set of equations, we get

$$(1 + \alpha N) \partial_x^2 \psi_1 = \left(1 + \frac{\alpha N}{c_e^2} \right) \partial_t^2 \psi_1 + \gamma_e \partial_t \psi_1 + f_1 - Nj, \quad (52a)$$

$$v_l^2 \partial_x^2 \psi_l = \partial_t^2 \psi_l + \gamma \partial_t \psi_l + f_l, \quad l = 2, \dots, N, \quad (52b)$$

where f_l are the cos transform images of $\sin(\phi_m + 2\pi R_m x/L)$. Applying then the Fourier transform over coordinate x , we obtain a set of ordinary differential equations

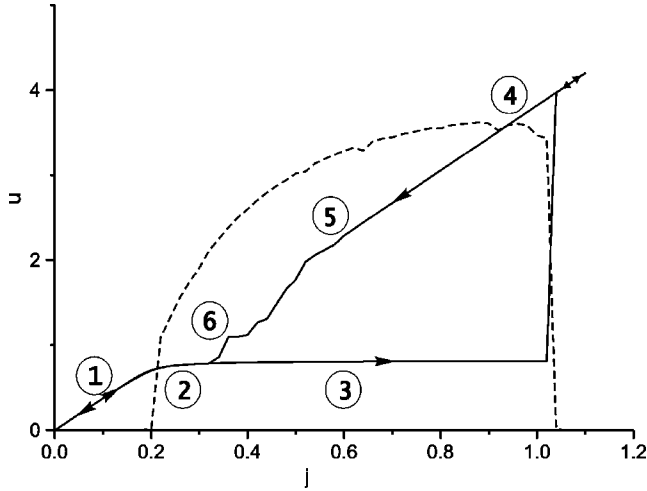


FIG. 11. CV curve of the four-layer system. See text for the parameters. Digits denote the CV regions corresponding to different vortex flow regimes (see Figs. 12–17). Dashed line shows the dependence of the first harmonic of the field amplitude on external current.

$$-k^2(1 + \alpha N)\tilde{\psi}_{1,k} = \left(1 + \frac{\alpha N}{c_e^2}\right)\ddot{\tilde{\psi}}_{1,k} + \gamma_e \dot{\tilde{\psi}}_{1,k} + \tilde{f}_{1,k} - NLj\delta(k), \quad (53a)$$

$$-k^2v_l^2\tilde{\psi}_{l,k} = \ddot{\tilde{\psi}}_{l,k} + \gamma\dot{\tilde{\psi}}_{l,k} + \tilde{f}_{l,k} \quad l=2, \dots, N \quad (53b)$$

where the point denotes the derivative over time. In order to calculate the Fourier transform, we use the standard fast Fourier transform (FFT) algorithm. We reduce this system to the set of first order differential equations and solve the latter by the fourth-order Runge-Kutta method. As a result, we build a current-voltage (CV) characteristic (Fig. 11) and field distributions φ_{nx} as functions of coordinate x and layer index n .

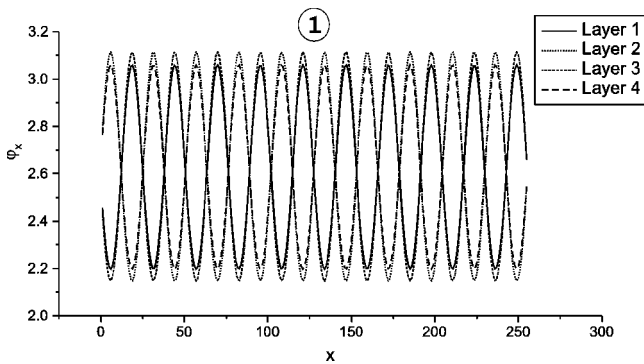


FIG. 12. The coordinate distribution of φ_{nx} , $n=1, \dots, 4$ at $j=0$. Vortices form a triangular lattice. Here and in the following figures the digit above plot denotes the region of CV curve where this distribution is established (see Fig. 11).

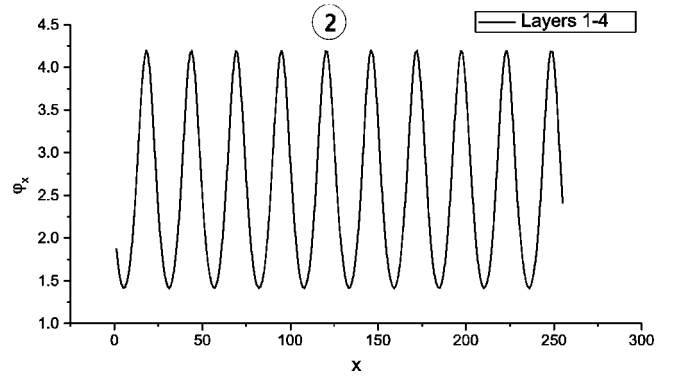


FIG. 13. The coordinate distribution of φ_{nx} , $n=1, \dots, 4$ at $j=0.22$. In-phase regime with a large amplitude of the alternate field component.

B. Results

Figure 11 shows the CV curve calculated in the numerical experiment. We measure the JVL velocity at a given external current j , which is varied from 0 to 1.1 with a step 0.02 forward and back. We use the following parameters: number of layers $N=4$, number of flux quanta in each layer $R=10$, length of the system $L=24$, $\alpha=0.1$, $\gamma=0.1$, $\Gamma=0$, $s=-0.07$, $c_e=0.6$. The parameters are chosen so that the characteristic velocity of the symmetric perturbation v_1 is the smallest of the characteristic velocities of all other perturbation modes v_l , $l=2, \dots, N$.

We now consider the CV characteristic of the system consisting of four layers (Fig. 11). At $j=0$ (starting point of the measurement) a static triangular JVL is formed (Fig. 12). When the current is increased, the lattice starts moving, keeping the triangular arrangement of vortices. At the point $j=0.22$ the transition to the in-phase regime takes place (Fig. 13). In this point of CV the JVL velocity is approximately equal to $u=0.737$, which is in a good agreement with analytical formula (49). As seen from Fig. 11, the amplitude of the first harmonic of the field in the in-phase regime is sharply increased to about half of the mean field value (Fig. 13). It indicates high efficiency of the ac/dc conversion rate in this regime. With a further increase of current the in-phase regime persists but vortices experience Lorentz contraction (Fig. 14). The ac/dc conversion rate remains high up to the point $j=1$. At $j=1$ the system changes the vortex flow regime to the one with a fast phase growth rate. The field distribution is not qualitatively changed in this point but the first harmonic amplitude sharply decreases (Figs. 11 and 15). When we decrease the current from $j=1.1$ the field oscillation amplitude gradually increases, and the in-phase regime persists. In the interval from $j=0.6$ to $j=0.32$ the CV curve exhibits a series of bends. Apparently, they are associated with the successive changes of stability conditions of asymmetric modes. As the JVL velocity is decreased, the asymmetric modes become unstable one by one due to the parametric instability. The typical distribution of φ_{xn} in this current interval is shown in Fig. 16. At $j=0.36$ the field distribution shows 12 maximums (Fig. 17) while we know that only 10 flux quanta are trapped into each junction. It means that the short-wave-length instabilities lead to a vortex-

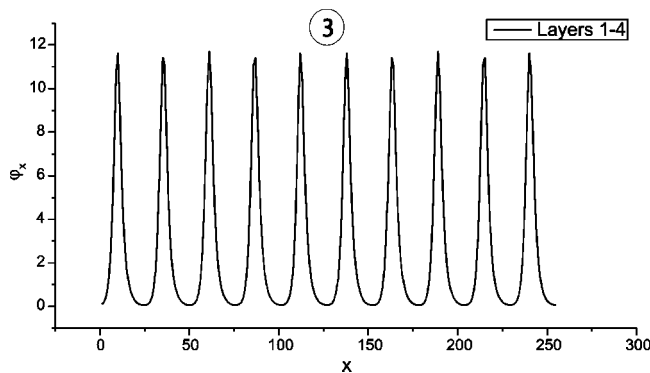


FIG. 14. The coordinate distribution of φ_{nx} , $n=1, \dots, 4$ at $j=0.6$. Lorentz contraction of the vortices.

antivortex pair nucleation in the system. By further decrease of j the pair is annihilated, the rectangular JVL is restored and, after the point $u=v'$, the in-phase regime turns into a triangular lattice.

The case when the characteristic velocity of symmetric perturbations is greater than the characteristic velocities of other modes is equivalent to the case of a multilayer system without any electromagnetic environment. The particular situation of two-layer system without electromagnetic environment was analyzed in Ref. 10. It was shown that the in-phase regime is stable only when the JVL velocity exceeds some critical value when the parametric instability becomes suppressed. Therefore, we do not expect any spontaneous establishing of the in-phase regime as we have observed above and do not perform a numerical experiment for that case.

One may come to several conclusions from the numerical experiment. First, the in-phase regime of the vortex flow is formed provided the symmetric mode of perturbations in the system is the slowest one, and this formation takes place at the JVL velocity calculated by formula (49). Second, at a relatively high JVL velocity the short-wave-length instability appears, leading to nucleation of vortex-antivortex pairs in the system. Finally, at high velocity the rectangular JVL is stable due to the parametric instability suppression. However, this regime of vortex flow is not promising for applications because the alternating component of the field is very low.

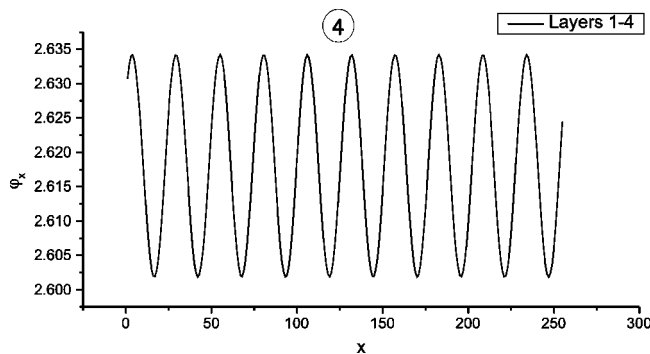


FIG. 15. The coordinate distribution of φ_{nx} , $n=1, \dots, 4$ at $j=0.96$ (reverse branch). In-phase regime with a small amplitude of the alternate field component.

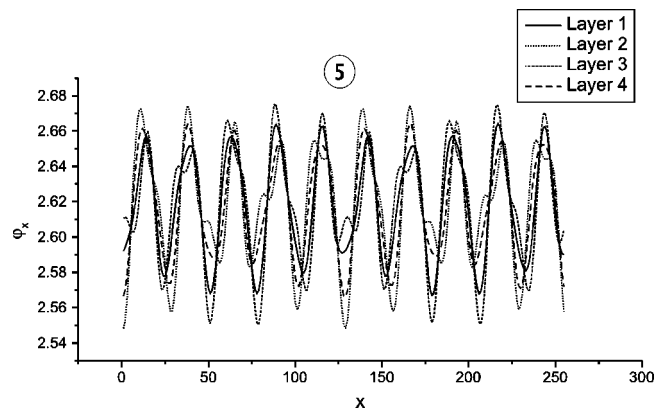


FIG. 16. The coordinate distribution of φ_{nx} , $n=1, \dots, 4$ at $j=0.6$ (reverse branch). The development of short-wave-length instabilities.

V. DISCUSSION AND SUMMARY

In order to achieve stability of the in-phase regime of vortex flow in a multilayer Josephson structure, it is necessary to slow down the symmetric mode of perturbations in the system. This deceleration must make the symmetric mode slowest compared to all other perturbation modes. Then the in-phase regime becomes absolutely stable in the interval of velocities from v' to v_1 .

Let us estimate the deceleration which is necessary to achieve stability of the in-phase regime. For typical parameter values of BSCCO $d'=12 \text{ \AA}$, $t=3 \text{ \AA}$,¹⁷ we have $v_{min} \approx 10^{-3}c$. As follows from the expression for v_1 (see Sec. III), in order to fulfill the condition $v_1 < v_{min}$ we must at least provide $c_e < v_{min}$. In order to reach such a slowing in a stripline, one should fill it with a dielectric with large ϵ . Dielectric function ϵ exhibits sharp peaks at frequencies close to resonances on intrinsic degrees of freedom such as optical phonons. It is also possible to use more complicated slow-wave system, for example, a periodic structure similar to that used in a traveling wave tube or in a backward wave tube. Due to the periodicity, the wave spectrum in this system has zone structure, and is characterized by presence of suppression bands. The cutoff frequencies are determined by resonant frequencies of the slow-wave system elements. By decrease of the resonant frequency one may significantly re-

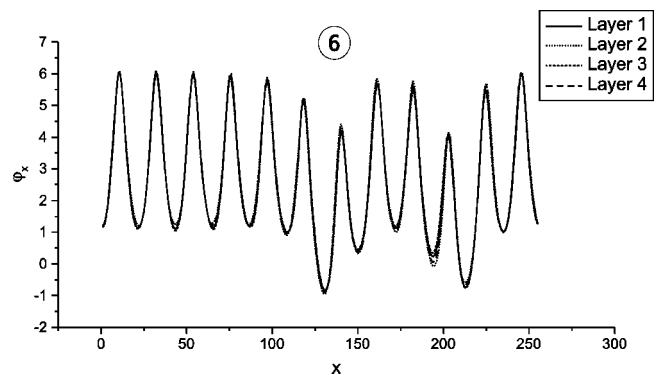


FIG. 17. The coordinate distribution of φ_{nx} , $n=1, \dots, 4$ at $j=0.36$ (reverse branch). Vortex-antivortex pair nucleation.

duce the phase velocity in the system. Another way to obtain the required deceleration is to engage intrinsic resonances in HTSC, for example, coupling via c -axis phonons.¹⁸ We emphasize once more that we choose a stripline only as a model of a slow-wave structure in our consideration.

As for niobium multilayers, their parameters such as superconducting and insulator layers' thicknesses, are controllable. Thus, they can be fabricated so that a stripline is sufficient to provide the necessary deceleration of the symmetric perturbation mode.

ACKNOWLEDGMENTS

This work has been supported by Russian Foundation for Basic Research (Grant Nos. 03-02-16533a, 02-02-16775a, and 03-02-06344mas) and by the RAS fundamental research program "Nonlinear Dynamics." The authors are grateful to N. Gress for assistance.

*Electronic address: chig@ipm.sci-nnov.ru

- ¹A. Barone and G. Paternò, *Physics and Applications of the Josephson Effect* (Wiley, New York, 1982).
- ²H. Kohlstedt, G. Hallmanns, I. P. Nevirkovets, D. Guggi, and C. Heiden, *IEEE Trans. Appl. Supercond.* **3**, 2197 (1993).
- ³R. Kleiner, F. Steinmeyer, G. Kunkel, and P. Müller, *Phys. Rev. Lett.* **68**, 2394 (1992); R. Kleiner and P. Müller, *Phys. Rev. B* **49**, 1327 (1994).
- ⁴H. B. Wang, L. X. Lou, J. Chen, P. H. Wu, and T. Yamashita, *Supercond. Sci. Technol.* **15**, 90 (2002).
- ⁵T. Nagatsuma, K. Enpuku, F. Irie, and K. Yoshida, *J. Appl. Phys.* **54**, 3302 (1983); T. Nagatsuma, K. Enpuku, K. Yoshida, and F. Irie, *ibid.* **56**, 3284 (1984); T. Nagatsuma, K. Enpuku, K. Sueoka, K. Yoshida, and F. Irie, *ibid.* **58**, 441 (1985).
- ⁶A. F. Volkov and V. A. Glen, *J. Phys.: Condens. Matter* **10**, L563 (1998).
- ⁷A. E. Koshelev and I. S. Aranson, *Phys. Rev. Lett.* **85**, 3938 (2000); A. E. Koshelev and I. Aranson, *Phys. Rev. B* **64**, 174508 (2001).
- ⁸K. Likharev, *Dynamics of Josephson junctions and circuits* (Gordon and Breach, New York, 1986).
- ⁹G. Filatrella, N. F. Pedersen, and K. Wiesenfeld, *Phys. Rev. E* **61**, 2513 (2000); G. Filatrella and N. F. Pedersen, *Physica C* **372–376**, 11 (2002).
- ¹⁰A. V. Chiginev and V. V. Kurin, *Phys. Rev. B* **66**, 052510 (2002).
- ¹¹S. Sakai, P. Bodin, and N. F. Pedersen, *J. Appl. Phys.* **73**, 2411 (1993).
- ¹²L. N. Bulaevskii, M. Zamora, D. Baeriswyl, H. Beck, and J. R. Clem, *Phys. Rev. B* **50**, 12831 (1994).
- ¹³T. Koyama and M. Tachiki, *Phys. Rev. B* **54**, 16183 (1996); S. N. Artemenko and A. G. Kobel'kov, *Phys. Rev. Lett.* **78**, 3551 (1997).
- ¹⁴D. A. Ryndyk, *Pis'ma Zh. Eksp. Teor. Fiz.* **65**, 755 (1997) [*JETP Lett.* **65**, 791 (1997)]; *Phys. Rev. Lett.* **80**, 3376 (1998); D. A. Ryndyk, *Zh. Eksp. Teor. Fiz.* **116**, 1798 (1999) [*JETP* **89**, 975 (1999)].
- ¹⁵N. Flytzanis, N. Lazarides, A. Chiginev, V. Kurin, and J. G. Caputo, *J. Appl. Phys.* **88**, 4201 (2000); C. Lee, *IEEE Trans. Appl. Supercond.* **1**, 121 (1991); C. Lee and A. Barfknecht, *ibid.* **2**, 67 (1992).
- ¹⁶D. W. McLaughlin and A. C. Scott, *Phys. Rev. A* **18**, 1652 (1978).
- ¹⁷R. Kleiner, P. Müller, H. Kohlstedt, N. F. Pedersen, and S. Sakai, *Phys. Rev. B* **50**, 3942 (1994).
- ¹⁸Ch. Helm, Ch. Preis, F. Forsthofer, J. Keller, K. Schlenga, R. Kleiner, and P. Müller, *Phys. Rev. Lett.* **79**, 737 (1997).